JOURNAL OF GEOPHYSICAL RESEARCH, VOL. 113, D24112, doi:10.1029/2008JD010404, 2008



# Trends and interdecadal changes of weather predictability during 1950s–1990s

Ruiqiang Ding,[1] Jianping Li,[1] and Kyung-Ja Ha[2]

Received 13 May 2008; revised 25 September 2008; accepted 10 October 2008; published 20 December 2008.

[1] To study the atmospheric predictability from the view of nonlinear error growth dynamics, a new approach using the nonlinear local Lyapunov exponent (NLLE) is introduced by the authors recently. In this paper, the trends and interdecadal changes of weather predictability limit (WPL) during 1950s–1990s are investigated by employing the NLLE approach. The results show that there exist significant trend changes for WPL over most of the globe. At three different pressure levels in the troposphere (850, 500, and 200 hPa), spatial distribution patterns of linear trend coefficients of WPL are similar. Significant decreasing trends in WPL could be found in the most regions of the northern midlatitudes and Africa, while significant increasing trends in WPL lie in the most regions of the tropical Pacific and southern mid-high latitudes. In the lower stratosphere (50 hPa), the WPL in the whole tropics all shows significant increasing trends, while it displays significant decreasing trends in the most regions of the Antarctic and northern mid-high latitudes. By examining the temporal variations of WPL in detail, we find that the interdecadal changes of WPL in most regions at different levels mainly happen in the 1970s, which is consistent with the significant climate shift occurring in the late 1970s. Trends and interdecadal changes of WPL are found to be well related to those of atmospheric persistence, which in turn are linked to the changes of atmospheric internal dynamics. Further analysis indicates that the changes of atmospheric static stability due to global warming might be one of main causes responsible for the trends and interdecadal changes of atmospheric persistence and predictability in the southern and northern mid-high latitudes. The increased sea surface temperature (SST) variability exerts a stronger external forcing on the tropical Pacific atmosphere that tends to enhance the persistence of tropical Pacific atmosphere. This process appears to be responsible for the increase of atmospheric predictability and persistence in the tropical Pacific since the late 1970s.

**Citation:** Ding, R., J. Li, and K.-J. Ha (2008), Trends and interdecadal changes of weather predictability during 1950s–1990s, *J. Geophys. Res.*, *113*, D24112, doi:10.1029/2008JD010404.

## 1. Introduction

[2] The atmosphere is a forced dissipative nonlinear system. On the assumption that external forces are bounded, the atmosphere attractor has been mathematically proved [*Li and Chou*, 1997; *Li and Wang*, 2008]. The predictability of atmospheric weather fluctuations is limited to 1–2 weeks due to the nonlinear and instability properties of the atmospheric flow [*Lorenz*, 1963, 1969]. Atmospheric predictability is found to vary obviously with time and it depends on the particular state of atmospheric flow patterns [*Lorenz*, 1965; *Legras and Ghil*, 1985; *Yoden and Nomura*, 1993]. Recent studies have found that extreme weather and climate events occur more frequently with the continuing global warming [*Zhai and Pan*, 2003; *Schär et al.*, 2004; *Webster et al.*, 2005]. To a certain extent, this will cause weather and climate forecasting to become more difficult. However, on the other hand, the increase of sea surface temperature (SST) variability over the tropical Pacific can enhance the atmospheric seasonal predictability [*Gu and Philander*, 1997; *Knutson et al.*, 1997; *Kang et al.*, 2006]. Due to the differences between the responses of atmospheric internal dynamics variability and external forcings to the global warming in different regions, interdecadal variability of atmospheric predictability shows different regional characteristics.

[3] *Goswami* [2004] demonstrated that the potential predictability of the Indian summer monsoon during 1980s and 1990s has decreased by almost a factor of two compared to its values during 1950s and 1960s, while the potential predictability of the summer climate over the central and eastern tropical Pacific has increased by a factor of two during the same period. *Nakaegawa et al.* [2004] pointed out that the forecast skill based on a 50-yr 10-member ensemble GCM integration with observed SST, has a

[1]State Key Laboratory of Numerical Modeling for Atmospheric Sciences and Geophysical Fluid Dynamics, Institute of Atmospheric Physics, Chinese Academy of Sciences, Beijing, China.
[2]Division of Earth Environmental System, Pusan National University, Busan, Korea.


0148-0227/08/2008JD010404$09.00

distinct positive trend since the 1950s, and this trend is consistent with the positive trend in the interdecadal timescale temporal variance of SST. *Kang et al.* [2006] investigated the seasonal predictability of global surface air temperature for the 100 years of 20th century international project (C20C) AGCM experiment and found that seasonal predictability has been increased since 1920s. It is further pointed out by *Kang et al.* [2006] that the increase of the seasonal predictability is related to the enhancement of SST variability over the tropical Pacific, which appears to be related to the global warming. *Wang et al.* [2007] showed that the skill of monthly temperature persistence forecast over China has significantly improved while the skill of monthly precipitation persistence forecast has slightly decreased from 1982 to 2005.

[4] The studies above mainly focus on the interdecadal changes of atmospheric predictability of monthly and seasonal means. However, up to now, few investigations have been performed investigating the interdecadal changes of weather predictability. It is shown that the interdecadal changes of atmospheric predictability of monthly and seasonal means are generally associated with the interdecadal changes of external forcings [*Goswami*, 2004; *Nakaegawa et al.*, 2004; *Kang et al.*, 2006], while the interdecadal changes of weather predictability are directly associated with the changes of internal dynamics variability of the atmosphere. Earth's surface is warmed by the greenhouse gas concentrations speculated to possibly change the internal dynamics variability of the atmosphere [*Tsonis*, 2004]. Therefore there is no doubt that the study of the interdecadal changes of weather predictability is very important for us to know about the effects of global warming on atmospheric predictability. In this paper we investigate the trends and interdecadal changes of weather predictability and shed light on the possible linkage of trend changes of weather predictability to global warming.

[5] In the previous studies of the interdecadal variability of the predictability of monthly and seasonal means, assessing the potential predictability based on observational data or ensemble GCM integration with prescribed SST is the most common method [*Goswami*, 2004; *Nakaegawa et al.*, 2004; *Kang et al.*, 2006]. However, this method is only applicable for the estimate of potential predictability of climate variability and cannot be used to study the problems of weather predictability. Although the weather forecast models can be used to estimate the skill of weather predictability, the state-of-the-art weather forecast models are not perfect and the simulation results are strongly model-dependent, especially in the tropics [*Kalnay*, 2003]. In addition, it seems to be a very difficult task to make the simulation using the weather forecast models for a very long period of time. Therefore it is necessary to introduce a new approach for quantifying the weather predictability limit (WPL).

[6] Recently, the first nonlinear local Lyapunov exponent (NLLE) [*Li et al.*, 2006; *Ding and Li*, 2007, 2008a] and the NLLE spectra of an $n$-dimensional nonlinear dynamical system [*Li and Wang*, 2008] are introduced. The first NLLE (hereafter NLLE) measures the nonlinear divergent rate of nonlinear system's trajectories with small initial perturbations or the nonlinear growth rate of initial errors of nonlinear dynamical model without linearizing the model's governing equations. With the NLLE and its derivatives, the limit of dynamic predictability in large classes of chaotic systems can be efficiently and quantitatively determined. Based on the atmospheric dynamic features, a reasonable algorithm has been provided to obtain the estimation of the NLLE and its derivatives by using the observational data [*Chen et al.*, 2006; *Ding and Li*, 2008b]. As a result, the NLLE approach can be successfully applied to the study of actual atmospheric predictability. In this paper, we will examine the trends and interdecadal changes of WPL using the NLLE approach. This paper is arranged as follows. Section 2 describes briefly the NLLE approach. Section 3 describes the data and analysis methods. Section 4 discusses the trends and interdecadal changes of WPL. The possible causes of trends and interdecadal changes of WPL are investigated in section 5. Finally, section 6 provides a summary and concluding remark.

## 2. Nonlinear Local Lyapunov Exponent (NLLE)

### 2.1. NLLE of an *n*-Dimensional System

[7] For an $n$-dimensional nonlinear dynamical system, its nonlinear perturbation equations are given by:

$$\frac{d}{dt}\boldsymbol{\delta}(t) = \mathbf{J}(\mathbf{x}(t))\boldsymbol{\delta}(t) + \mathbf{G}(\mathbf{x}(t), \boldsymbol{\delta}(t)), \tag{1}$$

where $\mathbf{x}(t) = (x_1(t), x_2(t), \cdots\cdots, x_n(t))^{\mathrm{T}}$ the reference solution, $\mathbf{J}(\mathbf{x}(t))\boldsymbol{\delta}(t)$ the tangent linear terms, and $\mathbf{G}(\mathbf{x}(t), \boldsymbol{\delta}(t))$ the high order nonlinear terms of the perturbations $\boldsymbol{\delta}(t) = (\boldsymbol{\delta}_1(t), \boldsymbol{\delta}_2(t), \cdots\cdots, \boldsymbol{\delta}_n(t))^{\mathrm{T}}$. The solutions of equation (1) can be obtained by numerically integrating it along the reference solution $\mathbf{x}(t)$ from $t = t_0$ to $t_0 + \tau$:

$$\boldsymbol{\delta}(t_0 + \tau) = \boldsymbol{\eta}(\mathbf{x}(t_0), \boldsymbol{\delta}(t_0), \tau)\boldsymbol{\delta}(t_0), \tag{2}$$

where $\boldsymbol{\eta}(\mathbf{x}(t_0), \boldsymbol{\delta}(t_0), \tau)$ is defined as the nonlinear propagator. Then the NLLE is defined as

$$\lambda(\mathbf{x}(t_0), \boldsymbol{\delta}(t_0), \tau) = \frac{1}{\tau}\ln\frac{\|\boldsymbol{\delta}(t_0 + \tau)\|}{\|\boldsymbol{\delta}(t_0)\|}, \tag{3}$$

where $\lambda(\mathbf{x}(t_0), \boldsymbol{\delta}(t_0), \tau)$ depends in general on the initial state in phase space $\mathbf{x}(t_0)$, the initial error $\boldsymbol{\delta}(t_0)$, and time $\tau$. The mean NLLE over attractor is given by

$$\overline{\lambda}(\boldsymbol{\delta}(t_0), \tau) = \langle\lambda(\mathbf{x}(t_0), \boldsymbol{\delta}(t_0), \tau)\rangle_N, \tag{4}$$

where $\langle\ \rangle_N$ denotes the ensemble average of samples of large enough size $N$ ($N \to \infty$). The mean relative growth of initial error (RGIE) can be obtained by

$$\overline{E}(\boldsymbol{\delta}(t_0), \tau) = \exp\big(\overline{\lambda}(\boldsymbol{\delta}(t_0), \tau)\tau\big). \tag{5}$$

Using the theorem proved by *Ding and Li* [2007], then we obtain

$$\overline{E}(\boldsymbol{\delta}(t_0), \tau) \xrightarrow{P} c(N \to \infty), \tag{6}$$

where $c$ can be considered as the theoretical saturation level of $\overline{E}(\boldsymbol{\delta}(t_0), \tau)$. Using the theoretical saturation level, the limit

of dynamic predictability can be quantitatively determined [*Li et al.*, 2006; *Ding and Li*, 2007, 2008a].

### 2.2. NLLE of Single Variable

[8] The definition of the NLLE in equation (3) actually aims to quantify the local error growth rate of the whole $n$-dimensional system, and the magnitude of error vector is measured by the norm of the $n$-dimensional vector. However, in a real situation, taking the case of atmosphere, for different variables such as the temperature, geopotential height, and precipitation, there might be different predictability. To quantify the error growth and predictability of different variables from an $n$-dimensional chaotic system, we define the NLLE of single variable $x_i (i = 1, 2, \cdots\cdots, n)$ on the basis of equation (3):

$$\xi_i(\mathbf{x}(t_0), \boldsymbol{\delta}(t_0), \tau) = \frac{1}{\tau} \ln \frac{|\delta_i(t_0 + \tau)|}{|\delta_i(t_0)|}. \tag{7}$$

Similarly, the mean NLLE and RGIE of variable $x_i$ can be obtained

$$\overline{\xi}_i(\boldsymbol{\delta}(t_0), \tau) = \langle \xi_i(\mathbf{x}(t_0), \boldsymbol{\delta}(t_0), \tau) \rangle_N. \tag{8}$$

$$\overline{\Phi}_i(\boldsymbol{\delta}(t_0), \tau) = \exp\left(\overline{\xi}_i(\boldsymbol{\delta}(t_0), \tau)\tau\right). \tag{9}$$

From equations (7)–(9), we get

$$\overline{\Phi}_i(\boldsymbol{\delta}(t_0), \tau) = \exp\left(\frac{1}{N} \sum_{j=1}^{N} \ln \frac{|\delta_{ij}(t_0 + \tau)|}{|\delta_{ij}(t_0)|}\right). \tag{10}$$

For the same initial error $\delta_i(t_0)$ of variable $x_i$, we have

$$\overline{\Phi}_i(\boldsymbol{\delta}(t_0), \tau) = \left(\prod_{j=1}^{N} |\delta_{ij}(t_0 + \tau)|\right)^{1/N} \Big/ |\delta_i(t_0)|. \tag{11}$$

For chaotic systems, as $\tau \to \infty$, $|\delta_{i1}(t_0 + \tau)|$, $|\delta_{i2}(t_0 + \tau)|$, $\cdots\cdots$, $|\delta_{iN}(t_0 + \tau)|$ will have the following independent identically distribution:

$$f(x) = \begin{cases} p(x), & 0 \le x \le a, \\ 0, & x < 0 \ \ or \ \ x > a, \end{cases} \tag{12}$$

where $a$ is a positive constant (because the chaotic attractor is confined to a finite region, $a$ is thought to be the maximum value of $\delta_i(t_0 + \tau)$), and $p(x)$ is a continuous function defined on a closed interval $[0, a]$. Using the Khinchine's Weak Law of Large Numbers [*Rose and Smith*, 2002], as $\tau \to \infty$, in the same way as equation (6), we can prove

$$\overline{\Phi}_i(\boldsymbol{\delta}(t_0), \tau) \xrightarrow{P} c_i \quad (N \to \infty), \tag{13}$$

where $c_i$ can be considered as the theoretical saturation level of $\overline{\Phi}_i(\boldsymbol{\delta}(t_0), \tau)$. Using the theoretical saturation level $c_i$, the limit of dynamic predictability of variable $x_i$ can be quantitatively determined.

[9] For systems whose equations of motion are explicitly known, such as Lorenz system, we can directly calculate the mean NLLE and the mean RGIE through the numerical integration of Lorenz system and its error evolution equations [*Ding and Li*, 2007, 2008a]. However, because the dynamic equations of the atmospheric motion are explicitly unknown, the NLLE and its derivatives cannot be directly calculated through the numerical integration of error evolution equations. In order to apply the NLLE approach to the study of actual atmospheric predictability, a reasonable algorithm is provided to obtain the estimation of the NLLE and its derivatives by using the observational data [*Chen et al.*, 2006; *Ding and Li*, 2008b]. The general idea of the algorithm is to estimate the NLLE by finding the analogues for each base date of the observations of one grid point, then investigating the evolution of the difference between the observations on the base date and their analogues. A brief description of the algorithm is given in Appendix A. Our results show that the algorithm is applicable. The NLLE approach has been used to investigate the temporal-spatial distributions of WPL [*Ding and Li*, 2008c], and the temporal-spatial distributions of the predictability limits of monthly and seasonal means [*Li and Ding*, 2008].

## 3. Data Used and Method of Analysis

[10] The data sets used in this study include the four times daily geopotential height fields and daily geopotential height and sea level pressure fields from the NCEP/NCAR reanalysis data (1948–2005) [*Kalnay et al.*, 1996], and monthly mean SST from version 2 of NOAA Extended Reconstructed SST data (1854–2005) [*Smith et al.*, 1996].

[11] By using the four times daily geopotential heights data, the variations of WPL can be analyzed based on the 11-yr moving window during 1948–2005. The annual mean WPL can be determined in the 11-yr window by employing the NLLE approach. The moving window moves forward every half year. The time axis indicates the middle year of the 11-yr moving window. Similarly, the variations of atmospheric persistence are also analyzed based on the 11-yr moving window during 1948–2005. Atmospheric persistence is measured by lag time (in day) for autocorrelation of daily geopotential height anomalies to reach the 0.05 significance level [*Trenberth*, 1985; *Reichler and Roads*, 2004]. The annual cycle and linear trend have been removed from daily geopotential heights data to obtain the daily geopotential height anomalies.

## 4. Trends and Interdecadal Changes of WPL

### 4.1. 500 hPa Geopotential Height Field

[12] Figure 1 shows the WPL anomalies of 500 hPa geopotential heights in different decades relative to the 1953–2000 average. It is shown that the variations of WPL in different decades have obvious regional characteristics. The positive anomalies of WPL appear over the tropical Pacific in the 1970s and persist till the 1980s and 1990s. In the most regions of southern midlatitudes, especially in the regions south of Australia, the WPL shows negative anomalies during 1950s and 1960s, but becomes positive anomalies from 1980s to 1990s. On the contrary, in the most regions of Asia-European Continent, northeastern

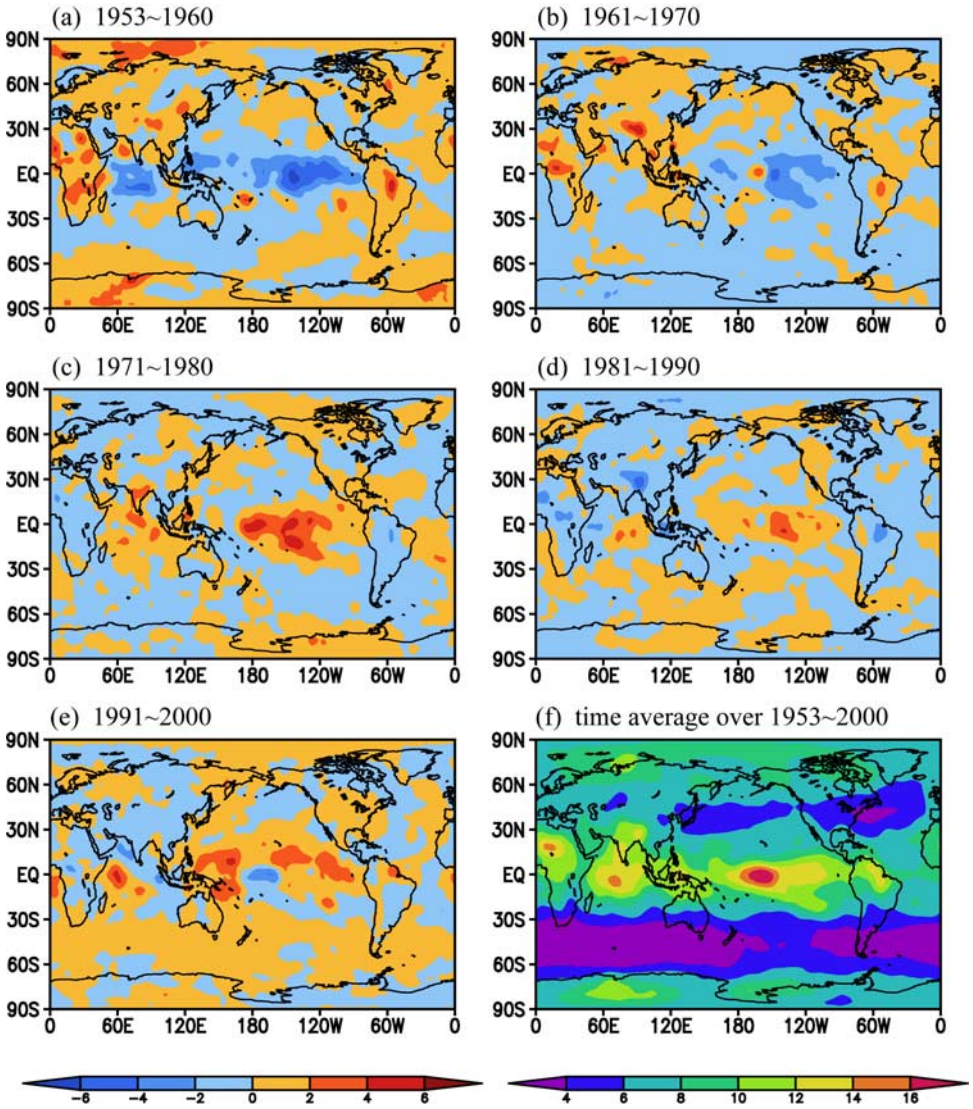


**Figure 1.** The WPL anomalies (in day) of 500 hPa geopotential heights in (a–e) different decades (color bar in the left) relative to (f) the 1953–2000 average (color bar in the right).

North America and Africa, the WPL becomes from positive anomalies to negative anomalies during 1950s and 1990s.

[13] To investigate the long-term trends of WPL, Figure 2b shows the linear trend coefficients of WPL of 500 hPa geopotential heights. Consistent with the results of Figure 1, the WPL shows significant increasing trends in the tropical Pacific and south of Australia, while it also shows significant decreasing trends in the most regions of Asia-European Continent, northeastern North America and Africa. In general, the WPL shows decreasing trends in the most regions of northern mid-high latitudes, while increasing trends could be found in the most regions of southern midlatitudes and equatorial regions, which can be seen clearly from the zonal average of the linear trend coefficients (Figure 3).

[14] We choose three regions with significant increasing trends and three regions with significant decreasing trends from Figure 2b, respectively. Figure 4 shows the temporal variation of the area-averaged WPL in each chosen region. It is evident that there are different characteristics of interdecadal variability in different regions. In the central-eastern China, the WPL has been decreasing from the early 1970s to mid-1980s, but shows a small increase from the late 1980s to 1990s (Figure 4a). The WPL in the southeastern Africa has been persistently decreasing from the 1960s to 1990s (Figure 4b). The WPL in the northeastern North America begins to decrease in the early 1960s and maintains at a very low level from the late 1970s to 1990s (Figure 4c). On the contrary, the WPL in the tropical eastern Pacific begins to increase in the early 1960s and maintains at a relative high level from the late 1970s to 1990s (Figure 4d). Different from the tropical eastern Pacific, the WPL in the tropical western Pacific increases from the early 1960s to mid-1970s, but then decreases slightly in the late 1970s and increases largely again in the mid-1980s and 1990s (Figure 4e). The WPL in the regions south of Australia has been persistently increasing from the 1960s to 1990s (Figure 4f).

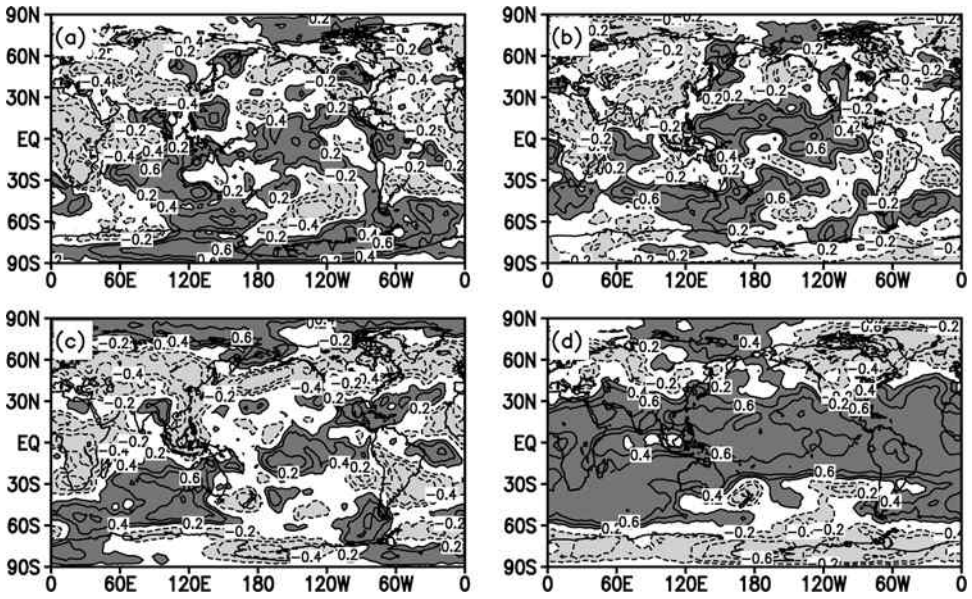


**Figure 2.** Linear trend coefficients of WPL of geopotential heights at (a) 850 hPa, (b) 500 hPa, (c) 200 hPa, (d) 50 hPa for the period 1953–2000. The values in the shaded areas are significant at the 0.05 level.

### 4.2. Geopotential Height Fields at Other Levels

[15] Besides the 500 hPa geopotential height field, the trends and interdecadal changes of WPL of geopotential heights at other levels (850, 200 and 50 hPa) are also investigated. It is found from Figure 2a that the spatial distribution pattern of linear trend coefficients at 850 hPa is very similar to that at 500 hPa. The WPL also exhibits significant decreasing trends in the most regions of the northern midlatitudes and Africa, and shows significant increasing trends in the most regions of southern mid-high latitudes and tropical Pacific. The temporal variation of WPL at different latitudes at 850 hPa can be seen from Figure 5. For example, the WPL at 60°N shows mostly positive anomalies before the mid-1970s, but shows mostly negative anomalies after the mid-1970s (Figure 5b). Similarly, the WPL in the region from 0°E to 80°E along the equator has mostly positive anomalies before the mid-1970s, but opposite change happens after the late-1970s. In the equatorial central-eastern Pacific (160°E∼120°W), the WPL shows mostly positive anomalies since the 1970s (Figure 5e). The WPL in the region from 100°E to 180°E along 60°S changes from the mostly negative anomalies to the mostly positive anomalies in the mid-1970s (Figure 5h).

[16] The distribution of linear trend coefficients at 200 hPa is also similar to that at 500 hPa, but some small differences exist between 200 hPa and 500 hPa (Figure 2c). For example, the WPL shows significant increasing trends in the most regions of Arctic at 200 hPa, while significant decreasing trends are found in the most regions of Arctic at 500 hPa. The regions of northern midlatitudes with significant decreasing trends at 200 hPa are wider than those at 500 hPa. From the temporal variation of the WPL at different latitudes at 200 hPa (not shown), the WPL at 80°N shows mostly positive anomalies before the mid-1980s, but shows mostly negative anomalies after the mid-1980s. The WPL at 60°N changes from the mostly positive anomalies to the mostly negative anomalies in the early 1970s. Same change at 40°N happens in the late 1970s. The WPL in the equatorial Africa has mostly positive anomalies before the 1980s, but opposite change happens after the 1980s. Same as 850 hPa and 500 hPa, the WPL in the equatorial central-eastern Pacific at 200 hPa also shows mostly positive anomalies since the 1970s.

[17] Linear trend coefficients at 50 hPa have more uniform spatial distribution than those at 850 hPa, 500 hPa and 200 hPa (Figure 2d). The WPL in the tropics at 50 hPa all shows significant increasing trends, while it shows significant decreasing trends in the most regions of Antarctic and northern mid-high latitudes. Specially, the WPL at 20°N and 20°S changes from the mostly negative anomalies to the mostly positive anomalies in the late 1970s (not shown). The WPL at the equator shows mostly negative anomalies from the mid-1960s to late 1970s, and shows mostly negative anomalies in other periods. The WPL in Antarctic

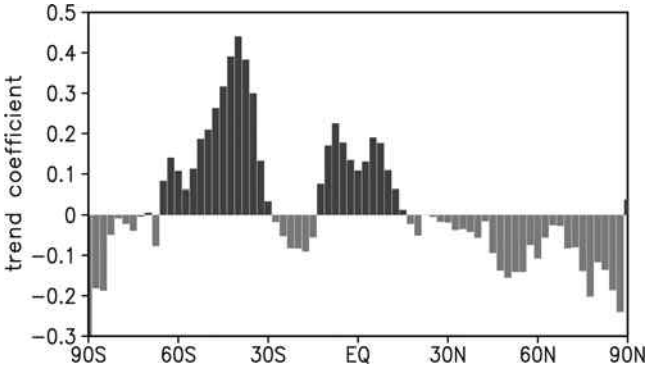


**Figure 3.** The zonal average of linear trend coefficients in Figure 2b.

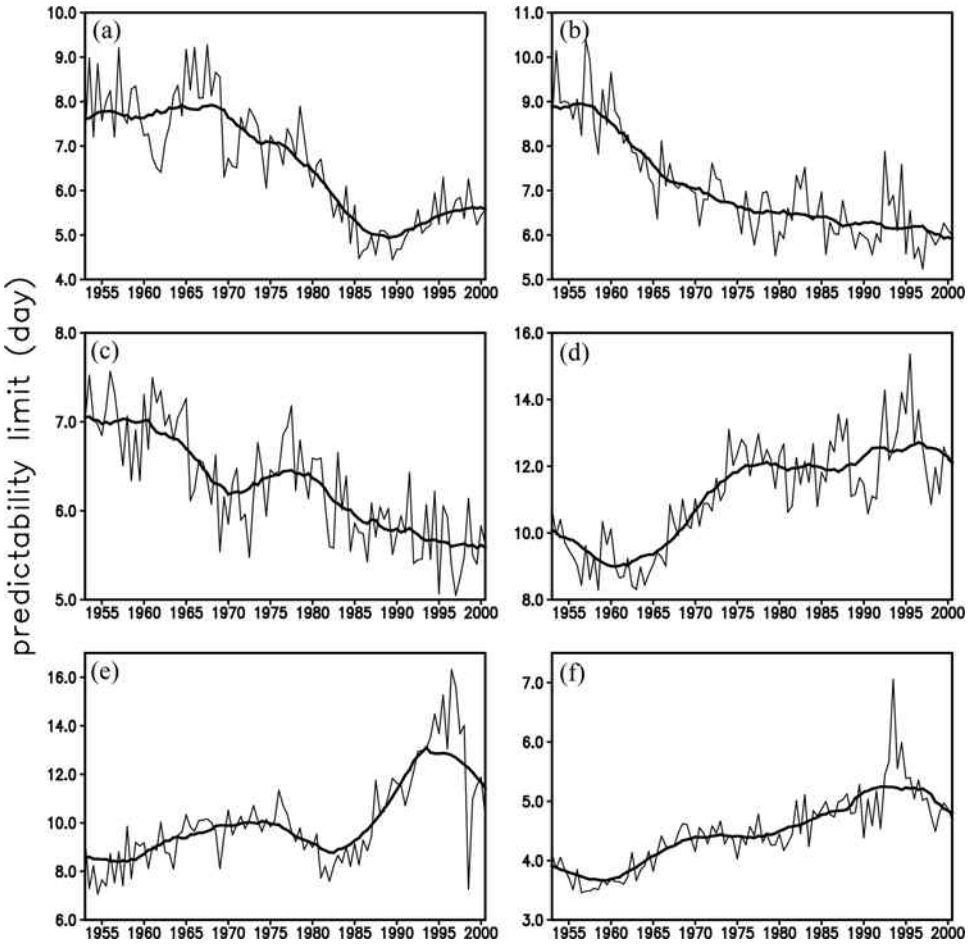


**Figure 4.** Temporal variations of the area-averaged WPL of geopotential heights in the six chosen regions at 500 hPa. Their 9-yr running mean series are indicated by the thick solid lines, respectively. Six chosen regions are (a) the central-eastern China (100–120°E, 25–35°E), (b) the southeastern Africa (35–45°E, 10–20°S), (c) the northeastern North America (60–70°W, 35–50°N), (d) the tropical eastern Pacific (80–160°W, 15°S–15°N), (e) the tropical western Pacific (120–180°E, 0–15°N), (f) south of Australia (120–180°E, 35–60°S).

has mostly positive anomalies before the late 1970s, but opposite change happens after the 1980s.

## 5. Possible Causes of Trends and Interdecadal Changes of WPL

### 5.1. Trends and Interdecadal Changes of Atmospheric Persistence of Daily Heights

[18] Atmospheric predictability correlates closely to the atmospheric persistence, which indicates the inherent long initial condition memory of the atmosphere [*Reichler and Roads*, 2004]. Therefore we explore whether the interdecadal variability of WPL is due to the atmospheric persistence. Figure 6 shows the linear trend coefficients of the atmospheric persistence of daily heights at 500 hPa. It is found that the spatial distribution of linear trend coefficients of the atmospheric persistence is very similar to that of WPL. The atmospheric persistence also exhibits significant decreasing trends in the most regions of the northern midlatitudes and Africa, and shows significant increasing trends in the most regions of tropical Pacific and south of Australia. Same six regions as those in Figure 4 are chosen to examine the temporal variation of the area-averaged atmospheric persistence in these six regions. Compared Figure 7 to Figure 4, we see that except the central-eastern China, atmospheric persistence in other five regions has similar interdecadal changes with atmospheric predictability limit. Over most of the globe, there are significant positive correlations between the atmospheric persistence and WPL on decadal timescales (Figure 8). From the similar interdecadal variability of the atmospheric persistence and WPL, it can be concluded that interdecadal changes of WPL might be directly related to those of the atmospheric persistence.

### 5.2. Further Analysis

[19] Under the global warming, obvious changes of atmospheric general circulation and the external forcings, such as SST, sea ice extent, etc. have been observed in the recent two decades [e.g., *Trenberth and Hurrell*, 1994; *Zhu et al.*, 2003; *Agudelo and Curry*, 2004; *Lindsay and Zhang*, 2005; *Xiao and Li*, 2007]. The changes of atmospheric general circulation and external forcings could modulate the dynamics of atmospheric internal variability, and in turn may change the atmospheric persistence and predictability.

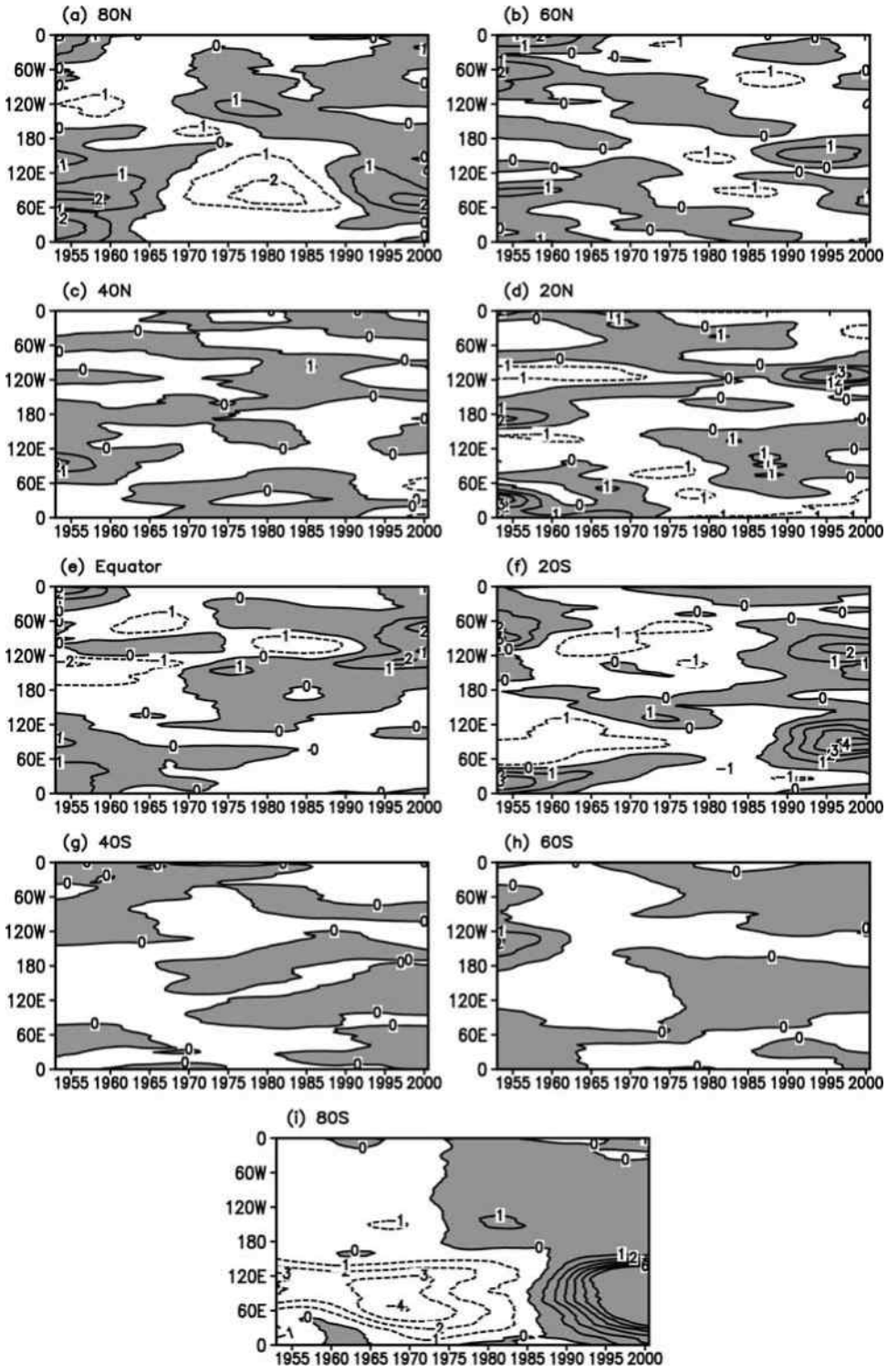


**Figure 5.** The time-longitude cross-sections of the WPL anomalies of geopotential heights (in day) relative to the 1953–2000 average at 850 hPa along nine different latitudes. The anomalies are shaded if greater than 0. The contour interval is 1.

Since 1958, observations show more warming at the surface than in the troposphere [*Angell*, 1999]. The difference between surface and tropospheric temperature therefore increases since 1958, which will lead atmospheric conditions to become more unstable. As a result, atmospheric predictability will get lower. Figure 9 shows the linear trend coefficients of the difference between surface and 500 hPa temperature. The temperature difference shows significant increasing trends in the most regions of northern mid-high latitudes, implying that atmospheric static stability in the most regions of northern mid-high latitudes decreases in recent decades. On the contrary, the temperature difference

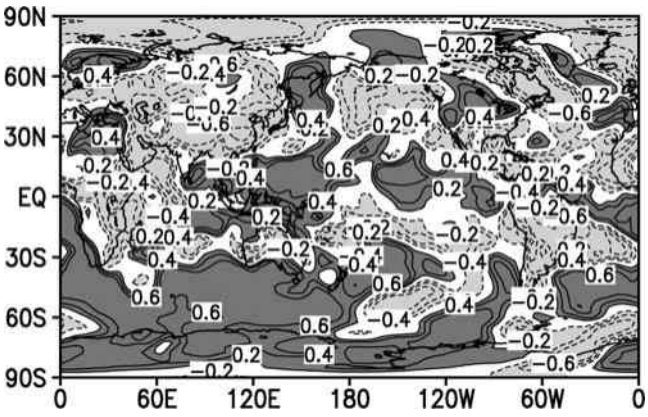


**Figure 6.** Same as Figure 2b, but for linear trend coefficients of atmospheric persistence of daily heights at 500 hPa.

shows significant decreasing trends in the most regions of southern mid-high latitudes, implying that atmospheric static stability in the most regions of southern mid-high latitudes increases in recent decades. Trend changes of temperature differences in the most regions of southern and northern mid-high latitudes are nearly consistent with those of WPL shown in Figure 2. The results suggest that the changes of atmospheric static stability due to global warming might be one of main causes responsible for the trends and interdecadal changes of atmospheric persistence and predictability in the southern and northern mid-high latitudes. However, the temperature difference shows significant increasing trends in the most regions of tropical Pacific, which is same as the trend changes of WPL. This implies that different from the mid-high latitudes, there may be other mechanisms responsible for the interdecadal changes of atmospheric persistence and predictability in the tropical Pacific.

[20] To gain some insight regarding the possible causes of the trends and interdecadal changes of atmospheric predict-

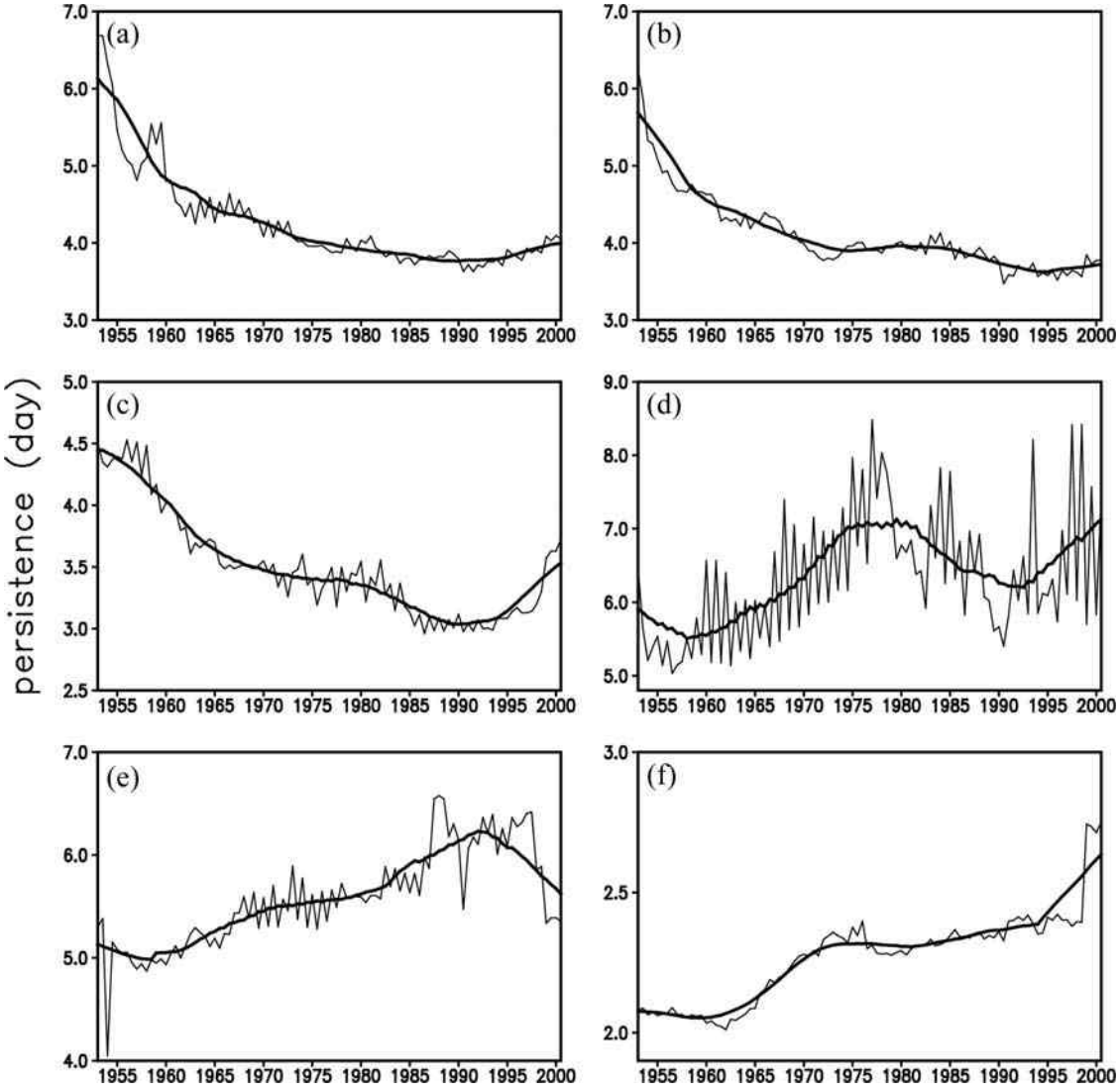


**Figure 7.** Same as Figure 4, but for the temporal variations of the area-averaged persistence of geopotential heights in the same six chosen regions at 500 hPa.

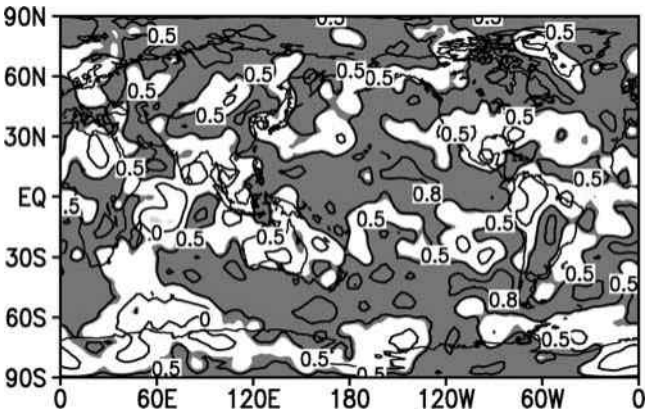


**Figure 8.** Correlation coefficients between 9-yr running mean series of atmospheric persistence and the WPL of geopotential heights at 500 hPa. The values in the shaded areas are significant at the 0.001 level.

ability in the tropical Pacific, a combined empirical orthogonal function (EOF) analysis was carried out using daily SST data and daily sea level pressure (Figure 10). The monthly SSTs are interpolated to daily values using cubic splines [*Perez et al.*, 2005]. The first EOF, explaining 20.9% of the variance, is quite distinct from the other EOFs and represents the response of the atmospheric anomalies to decadal ENSO variability. It is shown that the PC1 undergoes a distinct decadal change during the late 1970s (Figure 10c). Compared with earlier period (1948–1975), the PC1 in the period 1980–2005 is significantly higher, which is consistent with the increase of WPL in the tropical eastern Pacific shown in Figure 4d. The decadal shift of PC1 is related to the increased frequency of ENSO after the late 1970s. The increased frequency of ENSO exerts a stronger external forcing on the tropical Pacific atmosphere that tends to enhance the persistence of tropical Pacific atmosphere. This process appears to be responsible for the increase of atmospheric predictability and persistence in the tropical Pacific since the late 1970s. In addition, the increase of WPL in the tropical eastern Pacific since the late 1970s is consistent with warm phase of the Pacific Decadal Oscillation (PDO) [*Mantua et al.*, 1997; *Zhang et al.*, 1997]. It is implied that the PDO also possibly contributes to high WPL in the tropical eastern Pacific since the late 1970s.

## 6. Summary and Discussion

[21] Based on the NLLE approach introduced by the authors recently, the trends and interdecadal changes of WPL are investigated by using the NCEP/NCAR reanalysis data for the period 1948–2005. The results show that there exists significant trend changes for WPL over most of the globe. At three different pressure levels in the troposphere (850 hPa, 500 hPa and 200 hPa), the spatial distribution patterns of linear trend coefficients of WPL are similar. Significant decreasing trends in WPL could be found in the most regions of northern midlatitudes and Africa, while significant increasing trends in WPL lie in the most regions of tropical Pacific and southern mid-high latitudes. In the lower stratosphere (50 hPa), the WPL in the whole tropics all shows significant increasing trends, while it shows significant decreasing trends in the most regions of Antarctic and northern mid-high latitudes. By examining the temporal variation of WPL in detail, we find that the interdecadal changes of WPL in most regions at different levels mainly happen in the 1970s, which is consistent with the significant climate shift occurring in the late 1970s.

[22] Trends and interdecadal changes of WPL are found to be well related to those of atmospheric persistence, which in turn is linked to the changes of atmospheric internal dynamics. Further analysis indicates that the decrease of atmospheric static stability due to global warming might be one of main causes responsible for the trends and interdecadal variability of atmospheric persistence and predictability in the northern mid-high latitudes. The increased SST variability exerts a stronger external forcing on the tropical Pacific atmosphere that tends to enhance the persistence of tropical Pacific atmosphere. This process appears to be responsible for the increase of atmospheric predictability and persistence in the tropical Pacific since the late 1970s.

[23] There are two caveats to this study. First, while the NCEP/NCAR reanalysis is one of the most used data sets in the climate community and constitutes the main database for this study, some cautions should be given when considering the atmospheric interdecadal changes. Some spurious interdecadal changes due to the observational discontinuities have been found in the NCEP/NCAR reanalysis data [*Kistler et al.*, 2001; *Inoue and Matsumoto*, 2004]. Further work should be performed to compare the results of interdecadal changes of atmospheric predictability with other reanalysis or observational data. Second, the NLLE approach may be applied to studies of atmospheric predictability by using the observational data, and demonstrates superiority in determining the limit of atmospheric predictability in comparison with numerical models. Enough data requirement is one limitation of the NLLE approach [*Ding and Li*, 2008b]. By examining the NLLE evolution, we find that the four times daily height data over an 11 year period is adequate for the estimate of the NLLE. As the distribution of WPL depends on season [*Ding and Li*, 2008c], it is possible that the regions with significant trends in WPL are different for different seasons. However, considering the data requirement of the NLLE approach, we only investigate the interdecadal changes of annual mean WPL. The

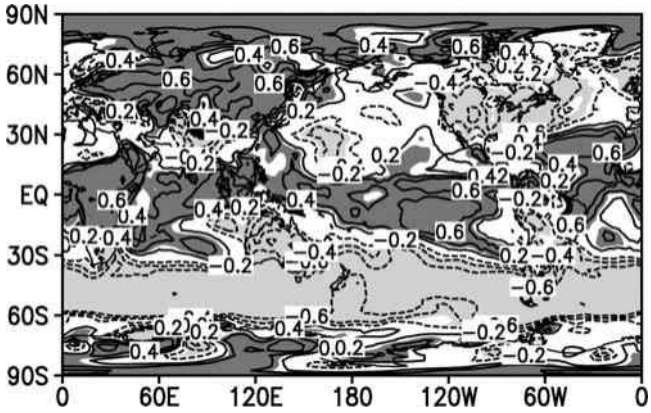


**Figure 9.** Same as Figure 2, but for linear trend coefficients of the difference between surface and 500 hPa annual mean temperature for the period 1953–2000.

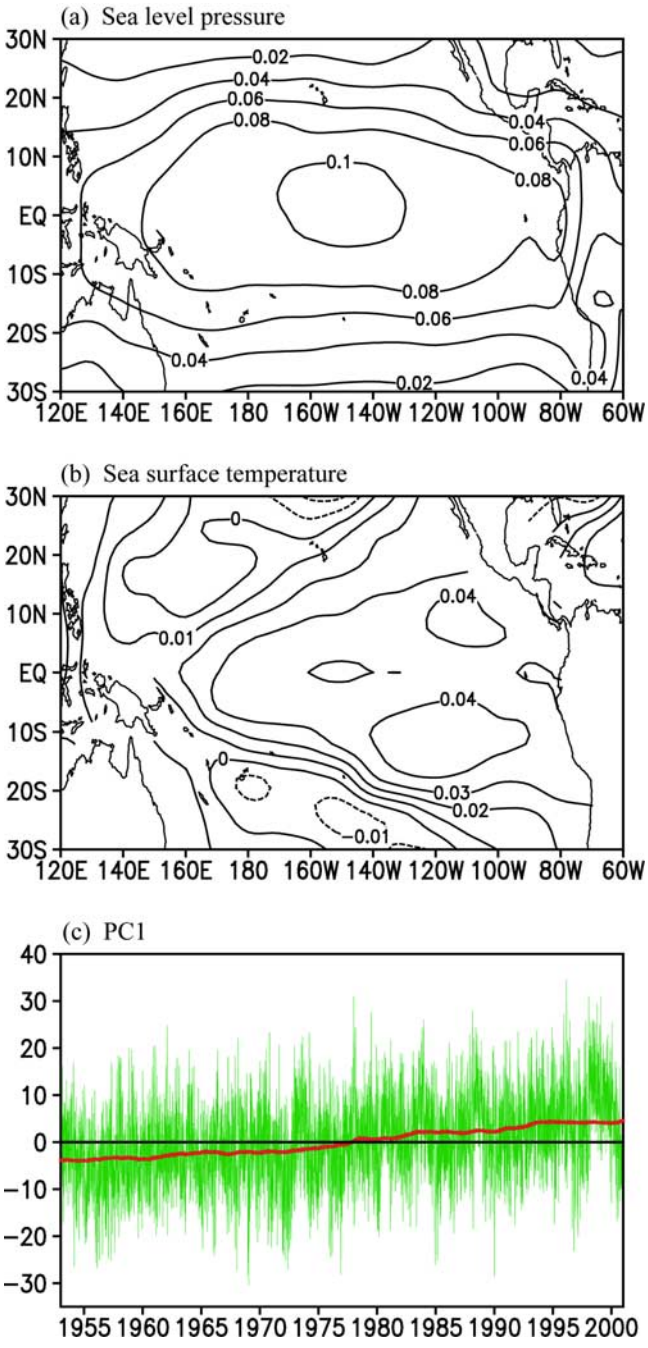


**Figure 10.** First combined EOF of (a) daily sea level pressure and (b) daily SSTs. (c) Time evolution of the PC1 is indicated by green line and its 9-yr running mean series are indicated by the thick red line.

comparison of interdecadal changes of WPL in different seasons is left for further study.

[24] Our results indicate that the responses of WPL to global climate changes are very complex. There are significant differences between different regions. Therefore it is very difficult to give a certain explanation for the interdecadal changes of the atmospheric predictability. Gaining further understanding of the causes of interdecadal changes of atmospheric predictability will require further study of the mechanisms determining the atmospheric predictability, and more generally about the shift in the atmospheric persistence and changes in atmospheric internal dynamics.

## Appendix A

[25] If the observational data of single variable of the atmosphere at one grid point has been obtained, the time series of the variable $x$ is given by $\{x(t_i), i = 1, 2, \cdots\cdots, m\}$ where $m$ represents the length of time series. To obtain the WPL of this variable, an algorithm that allow the estimation of the mean NLLE and the mean RGIE from the observational time series is given by the following steps.

[26] Step 1. Taking $x(t_1)$ as the reference point, we first try to find the local neighbor point $x(t_j)$ $(j \neq 1)$ of the reference point from the data set. As is well known, there exists a pronounced annual cycle in the atmosphere system because of the seasonal march of solar radiation. Two points at the almost same time of different year might have similar dynamic features, probably implying that one point is close to the other one in the phase space. We may search for the neighborhood of the reference point from all points occurring within the nearly same time of different year (for example, plus or minus 5 days from $t_1$ for four times daily observational data). We assume that the evolutions of two points (from $t_1$ to $t_k$) are analogous in a very short time if they are analogous at the initial time. The short time length from $t_1$ to $t_k$ is dependent on the timescale we are interested in. We find by experiment that the time length can be determined as 1/10 to 1/5 of the predictability limit of the timescale we are interested in. For the weather predictability considered in this paper, the time length is taken as 1 day for four times daily observational data. The root-mean-square distance (RMSD) between two points $x(t_1)$ and $x(t_j)$ during the short time $t_1$ to $t_k$ is given by

$$D = \sqrt{\sum_{i=0}^{k-1} \left(x(t_{1+i}) - x(t_{j+i})\right)^2 / k} \tag{A1}$$

The nearest neighbor $x(t_j)$ (hereafter $x'(t_1)$) of the reference point $x(t_1)$ can be chosen from all points occurring within the nearly same time of different year as $t_1$ only if the RMSD $D$ is minimum. The initial distance between $x(t_1)$ and $x'(t_1)$ is denoted as

$$L(t_1) = |x(t_1) - x'(t_1)|. \tag{A2}$$

[27] Step 2. At the time $t_n = t_1 + (n - 1)\Delta T$ $(n = 2, 3, \cdots\cdots)$ where $\Delta T$ is the minimum interval of time series, $x(t_1)$ will evolve into $x(t_n)$ along the reference trajectory, and $x'(t_1)$ will evolve into $x'(t_n)$. The initial difference $L(t_1)$ will become:

$$L(t_n) = |x(t_n) - x'(t_n)|. \tag{A3}$$

The growth rate of initial error during the time $t_n - t_1$ is

$$\xi_1(t_n) = \frac{1}{t_n - t_1} \ln \frac{L(t_n)}{L(t_1)}. \tag{A4}$$

With $n$ gradually increasing, we can obtain the variation of $\xi_1(t_n)$ as a function of evolution time $t_n$.

[28] Step 3. Taking $x(t_2)$ as the reference point, repeating the steps 1 and 2 above, we can get the variation of $\xi_2(t_n)$ as a function of evolution time $t_n$.

[29] Step 4. The above procedure is repeated until the reference trajectory has traversed the entire data file, at which point we estimate the mean NLLE,

$$\overline{\xi}(t_n) = \frac{1}{N}\sum_{i=1}^{N}\xi_i(t_n), \quad (n = 2, 3, \cdots\cdots) \tag{A5}$$

where $N$ ($N < m$) is the total number of the reference points on the reference trajectory.

[30] Step 5. From the equations (A4) and (A5), we can get the approximation of the mean RGIE,

$$\overline{\Phi}(t_n) = \exp\left(\overline{\xi}(t_n)t_n\right), \quad (n = 2, 3, \cdots\cdots) \tag{A6}$$

By investigating the evolution of $\overline{\Phi}(t_n)$ with $t_n$ increasing, we can estimate the mean predictability limit of variable $x$ at one local observation point.

[31] **Acknowledgments.** We wish to thank the anonymous reviewers for helpful comments and suggestions. We thank Prof. M. Mu for many useful comments and for his help with mathematics. This work was supported jointly by the 973 program (2006CB403600), NSFC Projects (40805022, 40675046), the Korea Meteorological Administration Research and Development Program under grant CATER 2008-4407, and the second stage of the Brain Korea 21 Project in 2008.

## References

Agudelo, P. A., and J. A. Curry (2004), Analysis of spatial distribution in tropospheric temperature trends, *Geophys. Res. Lett.*, *31*, L22207, doi:10.1029/2004GL020818.

Angell, J. K. (1999), Comparison of surface and tropospheric temperature trends estimated from a 63-station radiosonde network, 1958–1998, *Geophys. Res. Lett.*, *26*, 2761–2764.

Chen, B. H., J. P. Li, and R. Q. Ding (2006), Nonlinear local Lyapunov exponent and atmospheric predictability research, *Sci. China D*, *49*, 1111–1120.

Ding, R. Q., and J. P. Li (2007), Nonlinear finite-time Lyapunov exponent and predictability, *Phys. Lett. A*, *364*, 396–400.

Ding, R. Q., and J. P. Li (2008a), Nonlinear local Lyapunov exponent and quantification of local predictability, *Chin. Phys. Lett.*, *25*, 1919–1922.

Ding, R. Q., and J. P. Li (2008b), Studies on atmospheric predictability by the new approach of nonlinear local Lyapunov exponent (in Chinese with English abstract), *Acta Meteorol. Sin.*, *66*, 347–359.

Ding, R. Q., and J. P. Li (2008c), The temporal-spatial distributions of weather predictability of different variables (in Chinese with English abstract), *Acta Meteorol. Sin.*, in press.

Goswami, B. N. (2004), Interdecadal change in potential predictability of the Indian summer monsoon, *Geophys. Res. Lett.*, *31*, L16208, doi:10.1029/2004GL020337.

Gu, D., and S. G. H. Philander (1997), Interdecadal climate fluctuations that depend on exchanges between the tropics and extratropics, *Science*, *275*, 805–807.

Inoue, T., and J. Matsumoto (2004), A comparison of summer sea level pressure over east Eurasia between NCEP-NCAR reanalysis and ERA-40 for the period 1960–99, *J. Meteorol. Soc. Jpn.*, *82*, 951–958.

Kalnay, E., et al. (1996), The NCEP/NCAR 40-year reanalysis project, *Bull. Am. Meteorol. Soc.*, *77*, 437–471.

Kalnay, E. (2003), *Atmospheric Modeling, Data Assimilation and Predictability*, pp. 216–218, Cambridge Univ. Press, Cambridge.

Kang, I. S., E. K. Jin, and K. H. An (2006), Secular increase of seasonal predictability for the 20th century, *Geophys. Res. Lett.*, *33*, L02703, doi:10.1029/2005GL024499.

Knutson, T. R., S. Manabe, and D. Gu (1997), Simulated ENSO in a global coupled ocean-atmosphere model: Multidecadal amplitude modulation and $CO_2$ sensitivity, *J. Clim.*, *10*, 138–161.

Kistler, R. E., et al. (2001), The NCEP/NCAR 50-year reanalysis: Monthly means CD-ROM and documentation, *Bull. Am. Meteorol. Soc.*, *82*, 247–267.

Legras, B., and M. Ghil (1985), Persistent anomalies, blocking and variations in atmospheric predictability, *J. Atmos. Sci.*, *42*, 433–471.

Li, J. P., and J. F. Chou (1997), Existence of atmosphere attractor, *Sci. China D*, *40*, 215–224.

Li, J. P., and R. Q. Ding (2008), Temporal-spatial distributions of predictability limit of short-term climate (in Chinese with English abstract), *Chin. J. Atmos. Sci.*, *32*, 975–986.

Li, J. P., and H. S. Wang (2008), Some mathematical and numerical issues in geophysical fluid dynamics and climate dynamics, *Commun. Comput. Phys.*, *3*, 759–793.

Li, J. P., R. Q. Ding, and B. H. Chen (2006), *Review and Prospect on the Predictability Study of the Atmosphere*, pp. 96–104, China Meteorol. Press, Beijing.

Lindsay, R. W., and L. Zhang (2005), The thinning of Arctic sea ice, 1988–2003: Have we passed a tipping point?, *J. Clim.*, *18*, 4879–4894.

Lorenz, E. N. (1963), Deterministic nonperiodic flow, *J. Atmos. Sci.*, *20*, 130–141.

Lorenz, E. N. (1965), A study of the predictability of a 28-variable atmospheric model, *Tellus*, *3*, 321–333.

Lorenz, E. N. (1969), Atmospheric predictability as revealed by naturally occurring analogues, *J. Atmos. Sci.*, *26*, 636–646.

Mantua, N. J., S. R. Hare, Y. Zhang, J. M. Wallace, and R. C. Francis (1997), A Pacific interdecadal climate oscillation with impacts on salmon production, *Bull. Am. Meteorol. Soc.*, *78*, 1069–1079.

Nakaegawa, T., M. Kanamitsu, and T. M. Smith (2004), Interdecadal trend of prediction skill in an ensemble AMIP-Type experiment, *J. Clim.*, *17*, 2881–2889.

Oseledec, V. I. (1968), A multiplicative ergodic theorem: Lyapunov characteristic numbers for dynamical systems, *Trans. Moscow Math. Soc.*, *19*, 197–231.

Perez, C. L., A. M. Moore, J. Zavala-Garay, and R. Kleeman (2005), A comparison of the influence of additive and multiplicative stochastic forcing on a coupled model of ENSO, *J. Clim.*, *18*, 5066–5085.

Reichler, T., and J. O. Roads (2004), Time-space distribution of long-range atmospheric predictability, *J. Atmos. Sci.*, *42*, 249–263, 61.

Rose, C., and M. D. Smith (2002), *Mathematical Statistics with Mathematica*, pp. 311–322, Springer-Verlag, New York.

Schär, C., P. L. Vidale, D. Lüthi, C. Frei, C. Häberli, M. A. Liniger, and C. Appenzeller (2004), The role of increasing temperature variability for European summer heat waves, *Nature*, *427*, 332–336.

Smith, T. M., R. W. Reynolds, R. E. Livezey, and D. C. Stokes (1996), Reconstruction of historical sea surface temperatures using empirical orthogonal functions, *J. Clim.*, *9*, 1403–1420.

Trenberth, K. E. (1985), Persistence of daily geopotential heights over the Southern Hemisphere, *Mon. Weather Rev.*, *113*, 38–53.

Trenberth, K. E., and J. W. Hurrell (1994), Decadal atmospheric-ocean variations in the Pacific, *Clim. Dyn.*, *9*, 303–309.

Tsonis, A. A. (2004), Is global warming injecting randomness into the climate system?, *Eos Trans. AGU*, *85*(38), 361, doi:10.1029/2004EO380002.

Wang, H. J., L. J. Chen, W. J. Li, P. Q. Zhang, and L. L. Liu (2007), Predictability of DERF on monthly mean temperature and precipitation over China, *Acta Meteorol. Sin.*, *65*, 725–732.

Webster, P. J., G. J. Holland, J. A. Curry, and H. R. Chang (2005), Changes in tropical cyclone number, duration, and intensity in a warming environment, *Science*, *309*, 1844–1846.

Xiao, D., and J. P. Li (2007), Spatial and temporal characteristics of the decadal abrupt changes of global atmosphere-ocean system in the 1970s, *J. Geophys. Res.*, *112*, D24S22, doi:10.1029/2007JD008956.

Yoden, S., and M. Nomura (1993), Finite-time Lyapunov stability analysis and its application to atmospheric predictability, *J. Atmos. Sci.*, *50*, 1531–1543.

Zhai, P. M., and X. H. Pan (2003), Trends in temperature extremes during 1951–1999 in China, *Geophys. Res. Lett.*, *30*(17), 1913, doi:10.1029/2003GL018004.

Zhang, Y., J. M. Wallace, and D. S. Battisti (1997), ENSO-like interdecadal variability: 1900–93, *J. Clim.*, *10*, 1004–1020.

Zhu, J. H., S. W. Wang, X. D. Zhang, Q. Z. Mu, and Z. H. Xie (2003), Basic modes of the general circulations under the global warming, *Prog. Nat. Sci.*, *13*, 417–421.

R. Ding and J. Li, State Key Laboratory of Numerical Modeling for Atmospheric Sciences and Geophysical Fluid Dynamics, Institute of Atmospheric Physics, Chinese Academy of Sciences, P.O. Box 9804, Beijing 100029, China. (ljp@lasg.iap.ac.cn)

K.-J. Ha, Division of Earth Environmental System, Pusan National University, 30 Jangjeon-dong, Geumjeong-gu, Busan 609-735, Korea. (kjha@pusan.ac.kr)